TOPICAL REVIEW — Low-dimensional nanostructures and devices

Topological insulator nanostructures and devices*

Xiu Fa-Xian(修发贤)† and Zhao Tong-Tong(赵彤彤)

State Key Laboratory of Surface Physics and Department of Physics, Fudan University, Shanghai 200433, *China*

(Received 31 July 2013)

Topological insulators' properties and their potential device applications are reviewed. We also explain why topological insulator (TI) nanostructures are an important avenue for research and discuss some methods by which TI nanostructures are produced and characterized. The rapid development of high-quality TI nanostructures provides an ideal platform to exploit salient physical phenomena that have been theoretically predicted but not yet experimentally realized.

Keywords: topological insulators, nanostructures, quantum spin Hall effect, Aharonov–Bohm effect

PACS: 61.46.–w, 62.25.–g, 64.70.kg **DOI:** 10.1088/1674-1056/22/9/096104

1. Introduction

Topological insulators are a new class of materials that have recently received substantial attention owing to their time-reversal-symmetry-protected surface states.[1–3] They are of interest for engineering applications because of special properties related to electrically insulating bulk states and the highly conducting and massless spin-helical surface states that are protected by the aforementioned time-reversal symmetry. Strong spin–orbit coupling of the surface carriers allows for the spin of a carrier to be completely determined by the direction of its momentum. A topological insulator (TI) material is marked by bulk states that have an energy bandgap and gapless surface states that are characterized by linear E–k dispersion, allowing surface carriers to have zero effective mass.[4] The band inversion that allows for the creation of these helical surface states is made possible by strong spin–orbit coupling, and the direction of momentum of a carrier on the surface is determined by its spin,[5] a phenomenon which could be useful for spintronics applications.[6]

More interesting is the protection of surface states by time-reversal symmetry. The existence of time-reversal symmetry means that the surface carriers can move with nearly no energy dissipation since perturbations, such as non-magnetic impurities that do not break the time-reversal symmetry, cannot scatter a carrier 180 degrees from the incident direction because they cannot invert the direction of the spin.[6]

However, in many applications the time-reversal symmetry of the system is broken by applying a magnetic field or adding magnetic dopants, and in those scenarios the surface carriers lose their massless character.[7] Topological insulator systems with broken time-reversal symmetry are predicted to give rise to Majorana fermions, each of which is its own antiparticle,[8] and a unique coupling of the electric and magnetic fields,[9,10] just to name two examples.

In this review, we will look further into the fundamental properties of topological insulators. We will also discuss the fabrication methods of TI nanostructures and elaborate on characterization methods that are needed to reveal the surface states. The applications of these materials in electronic and spintronic devices, both with and without time-reversal symmetry, will be explored. Special emphasis is placed on the importance of nanostructures when studying and exploiting the properties of topological insulators because of their large surface-to-volume ratios and high crystallinity. Finally, the current progress of making a variety of the TI nanostructures will be reviewed and a perspective on future developments is provided.

2. Topological insulators

2.1. Topological order

Phases of matter like topological insulators are examples of topologically ordered states that are not describable by a Landau approach to symmetry breaking with order parameters.[11] Typically, phases of matter, such as ferromagnetism, can be described by the breaking of some existing symmetry in the system. For the case of ferromagnetism, the rotational symmetry of the system in spin space is symmetric in the paramagnetic phase, with the order parameter (the magnetization) being zero.[12] However, below a critical temperature the symmetry is broken and the order parameter is non-zero. For a ferromagnetic material, the spin symmetry is broken in one direction in spin space and the amount of symmetry breaking is described by the magnetization of that region of space. Topologically ordered phases, however, cannot be described by symmetry breaking. An ordinary band insulator cannot have the parameters of its Hamiltonian continuously

*Project supported by the National Young 1000 Talents Plan of China and the Pu Jiang Talent Plan in Shanghai City, China.

†Corresponding author. E-mail: faxian@fudan.edu.cn

© 2013 Chinese Physical Society and IOP Publishing Ltd

adjusted to obtain the band structure of a topological insulator, without closing the bulk bandgap.[8]

2.2. Quantum Hall and spin quantum Hall effects

The quantum Hall (QH) state, discovered in 1980,[13] was the first experimental example of a topologically ordered state that is not describable using the theory of spontaneously broken symmetry.[11] By applying a strong magnetic field perpendicular to the surface of a semiconducting thin film at low temperature, the QH state can be observed.[10] The state is characterized by maintaining the energy gap in the interior of the semiconductor sample while giving rise to a low-dissipation current with quantized conductance on the edge of the sample. The conductance is quantized in integer units of e^2/h, where e is the electric charge and h is Planck's constant.[10]

The low-dissipation nature of the edge current arises from the topological robustness of the state, which forces the current to persist in only one direction, causing edge-state electrons that encounter impurities to move past the impurities (instead of being scattered backwards), leading to an increase in resistance. For an impurity to backscatter an edge-state electron, the electron must be scattered to the opposite edge of the sample, where the electron's momenta have the sign opposite that of the original surface electrons.[10] Despite the potential usefulness of low-dissipation edge currents, the QH state is not very practical for devices, as strong magnetic fields and low temperature are needed for the state to exist. However, there is another topologically ordered state known as the quantum spin Hall (QSH) state that is in many ways like the QH state, although the edge currents are spin currents rather than charge currents.[14]

In the QSH state, low-dissipation currents exist on the sample edge, just as in the QH state. However, unlike the QH state, no applied magnetic field is needed, and therefore the QSH state also has time-reversal symmetry. Spin–orbit coupling takes the place of an applied magnetic field in the QSH state and because of the time-reversal symmetry the surface currents move in two directions on the edge wherein the spin-up particles move in one way (either clockwise or counterclockwise) and the spin-down particles move along the edge in the opposite direction.[10,15] Like the QH state, the currents are low-dissipation, as the direction that an electron is moving along is determined by the direction of its spin, and non-magnetic impurities are capable of changing the direction of momentum of a charge carrier but not the orientation of its spin. Therefore, for a spin-up electron to backscatter 180° off a non-magnetic impurity, it would need to be transferred to the opposite edge where spin-up electrons are moving in the direction opposite the direction the electron was initially moving.[10]

The edge states of a QSH sample are topologically robust, as the features of low-dissipation currents and time-reversal symmetry persist so long as the surface is perturbed only by non-magnetic impurities. The energy-dispersion relation of a QSH sample has a crossing of edge states at $k = 0$. Around this point, the edge states are linear for both branches of states and so the surface carriers are known as Dirac electrons, as they obey the relativistic Dirac equation for a massless relativistic particle.[16] In these ways, the QSH state is synonymous with a two-dimensional topological insulator.[10]

2.3. Surface states of topological insulators

The term "topological insulator" has its origin in the study of topology in mathematics. A central concept of topology is that of a homeomorphism.[17] Two objects are homeomorphic if either object can be continuously transformed into the other object. Each system has a topological invariant which is a number that does not change when the continuous transformations between two objects are taking place. For geometric objects in Euclidian space, the topological invariant is the number of holes that appear in an object.[17] Thus, a sphere is homeomorphic to an ellipsoid because one can be continuously transformed into the other. However, a donut shape is not homeomorphic to a sphere as the donut has one hole that cannot be removed by a continuous transformation.[17]

Electronic wavefunctions can also be described by a topological invariant, and as in the case of geometric objects, certain wavefunctions cannot be continuously transformed into others. The surface state is the physical manifestation of the topological invariant changing between the region of space occupied by both a trivial insulator and a topological insulator that have states with non-homeomorphic wavefunctions. Only through a non-continuous phase transition can a topological insulator become a trivial insulator.[6]

The surface states of a topological insulator have a helical Dirac cone energy dispersion relation, which is the three-dimensional analogue of the two crossing linear dispersion curves for the QSH state. The existence of the massless Dirac cone surface states within the bulk energy band gap is due to the band inversion caused by strong spin–orbit coupling.

Typically, in semiconductors, the valence band is formed from the p orbitals of the constituent atoms while the conduction band is formed from the s orbitals. In a TI material, strong spin–orbit coupling breaks the degeneracy of the p-band states. The stronger the coupling is, the larger the energy gap that exists between the p-band states. If the coupling is strong enough, the $p_{3/2}$ states can move to a higher energy than the s-orbital band, leading to an inversion of the bands and a nearly linear dispersion curve for the surface states around $k = 0$.[5] Since spin–orbit coupling is a relativistic effect, band inversion is more likely to occur for heavier atoms where the electrons' motion is relativistic and the velocity-dependent spin–

orbit coupling is not negligible, and we see that the elements that make up many known topological insulators (e.g., Bi, Sb, Te) are relatively heavy.[10]

The first TI system to be discovered consisted of quantum wells of mercury telluride (HgTe) between layers of cadmium telluride (CdTe). It was predicted by Bernevig, Hughes, and Zhang,[18] but was not observed experimentally until 2007.[19] The amount of band inversion can be controlled by varying the thickness of the HgTe well. At a thickness of ~ 6.5 nm, a band inversion will happen in the HgTe quantum well, leading to topological surface states protected by time-reversal symmetry.[10]

With the application of a magnetic field or the introduction of magnetic impurities into the material, time-reversal symmetry can be broken in a TI system. This leads to the opening of a surface energy gap,[7,20] and because the bands are no longer linearly dispersed, the surface electrons acquire a mass. While massless surface states may be useful for low-dissipation transport of spin, many applications of TIs with broken-time reversal symmetry have been proposed, and these will be discussed in Section 3.

2.4. Current research

Since the first experimental observation of topological surface states in HgTe quantum wells in 2007, many other compounds have been found to be topological insulators. The most commonly studied examples are Bi_2Se_3, Bi_2Te_3, and Sb_2Te_3, as well as ternary compounds made from these elements.[21,22] The spectra taken from angle-resolved photoemission spectroscopy (APRES) measurements confirm that these compounds have helical Dirac surface states.[4,23,24]

Despite their name, TIs are not good electrical insulators, and all known TI materials have band gaps of less than 0.4 eV. Therefore, even for very intrinsic samples, the bulk contribution to the total conduction tends to overwhelm the contribution from the surface states, even at relatively low temperatures. Therefore, much work has been done to separate the contributions of the bulk and the surface to conduction in transport experiments.[20,25] Some effort has gone into material doping and electrical gating to lower the bulk carrier density. However, there are other issues whose resolution might increase the visibility of the surface states in TIs.

One attractive direction in the research is the use of nanostructures, wherein the ratio of surface area to volume is much higher than in bulk materials; so the total conduction from the bulk region is lower, allowing observation of the surface states in certain transport measurements.[26,27] In topological insulator nanostructures, oscillatory behavior of the resistance with varying applied magnetic field, due to the Aharanov–Bohm effect and Shubnikov–de Haas oscillations, can be used to help isolate the conduction of the surface from that of the bulk. Both effects will be discussed in Section 5.

3. Applications of topological insulators

3.1. Systems with time-reversal symmetry

In a topological insulator system without an applied magnetic field and without magnetic impurities, time-reversal symmetry exists. In this case "U"-turn scattering of the massless surface carriers is strongly suppressed, as the spin and momentum direction are locked together, and non-magnetic impurities can change the direction of momentum but not the orientation of the spin. As a result, low-dissipation spin current can exist on the surface, although significant energy dissipation may still exist in the bulk.

3.2. Systems without time-reversal symmetry

As mentioned previously, the time-reversal symmetry in TIs can be broken by applying a magnetic field or by adding magnetic impurities and cooling the sample below the temperature needed for magnetic ordering. There are many proposed applications for magnetically-doped TIs including a quantized conductance on the surface in units half as large as in the quantum Hall effect, known as the anomalous quantum Hall (AQH) effect, a novel electric and magnetic field coupling known as the magnetoelectric effect, the creation of fermions that act as their own antiparticle at the interface of a TI with a superconductor, which are called Majorana fermions,[28] an image magnetic monopole,[29] and a topological contribution to the Kerr and Faraday angles for incident polarized light.[30] We will discuss each of these effects in turn.

3.2.1. Anomalous quantum Hall effect

The anomalous quantum Hall (AQH) effect is much like the quantum Hall (QHE) except that a voltage transverse to the applied electric current in a sample appears even without the application of a magnetic field. The effect of the magnetic field in the QH effect is replaced by spin–orbit coupling of the charge carriers' momentum with their spin in an AQH insulator.[31] Reminiscent of the QH effect, breaking of the time-reversal symmetry with a magnetic field allows for the propagation of current along the sample edge.

Moreover, the conductance of this current is quantized in integer multiples of e^2/h in the QH effect. Likewise, the conductance in an anomalous quantum Hall state is expected to be quantized as $\sigma_{\mathrm{Hall}}=(2n+1)\,e^2/2h$ where n is an integer.[32] For example, in the topological insulator Bi_2Se_3, where there is one surface Dirac cone, we expect that $n=0$ so that $\sigma_{\mathrm{Hall}}=e^2/2h$. However, quantized conductance has not yet been observed in TI samples. The quantized AQHE is thought to be responsible for an interesting coupling between the electric and magnetic fields in TI samples.

3.2.2. Magnetoelectric effect

The magnetoelectric effect is described as an effect where a magnetic field applied in a magnetically doped topological insulator or in a topological insulator film that is in close proximity to a ferromagnetic film induces a net electric dipole moment, and conversely, an applied electric field will induce a net magnetic dipole moment.[9,11] The subject is often referred to as axion electrodynamics, as the term added in the action has the same form as a term which describes the interaction of a hypothetical axion field with the electromagnetic field in elementary particle physics.[8] In both cases the normal electromagnetic Lagrangian (density) L obtains an extra additive term,

$$\Delta\mathscr{L} = \theta(e^2/2\pi h)\boldsymbol{E}\cdot\boldsymbol{B},$$

where $\theta = 0(\mathrm{mod}\,2\pi)$ in ordinary insulators, $\theta = \pi(\mathrm{mod}\,2\pi)$ in a topological insulator, $\boldsymbol{E}$ and $\boldsymbol{B}$ are the electric field and magnetic flux density, respectively. It should be noted that θ itself has no direct effect on the electrodynamics as only the total derivative of θ is present in the equations of motion. At a magnetically gapped interface where the value of θ changes by $\Delta\theta$, however, the Hall surface conductivity is given by $\sigma = \Delta\theta(e^2/2\pi h)$.[8] We see that at the interface between a trivial insulator and a TI, $\Delta\theta = \pi$ and the value of the conductance agrees with the value associated with the anomalous quantum Hall state discussed previously.

The additional term in the Lagrangian leads to the relations (in Gaussian units)

$$\boldsymbol{D}=\boldsymbol{E}+4\pi\boldsymbol{P}-2\alpha\boldsymbol{P}_3\boldsymbol{B}, \quad \boldsymbol{H}=\boldsymbol{B}-4\pi\boldsymbol{M}+2\alpha\boldsymbol{P}_3\boldsymbol{E},$$

where $\boldsymbol{D}$ is the electric flux density, $\boldsymbol{H}$ is the magnetic field, and $\boldsymbol{P}$ and $\boldsymbol{M}$ are the polarizability and magnetization, respectively. Here, $\boldsymbol{P}_3 = 0$ for ordinary insulators, and $\boldsymbol{P}_3 = \pm 1/2$ in topological insulators.[29]

This is related to the AQH effect. If a cylindrical TI with a magnetically gapped surface has an electric field $\boldsymbol{E}$ pointing along the axis of the cylinder, then the azimuthal surface Hall current $(e^2/2h)|\boldsymbol{E}|$ gives rise to an overall magnetization $\boldsymbol{M}=\alpha\boldsymbol{E}$ where $\alpha=e^2/2h$.[8] However, there are several difficulties that must be dealt with in order to view the magnetoelectric effect in real materials. First, the carriers in the bulk must be suppressed. Second, in many cases an insulating ferromagnetic layer with magnetization normal to the interface must exist. Lastly, the Fermi energy must be adjusted so that it lies within the small energy gap in the surface states.[33] The first problem can be dealt with, for instance by using electrical gating, but the last two problems remain difficult at the moment.

3.2.3. Majorana fermions

Recently, the interface of TIs with a certain class of superconductors has been predicted to give rise to an electronic excitation known as a Majorana fermion, which is a particle that is its own antiparticle.[28] In three dimensions, indistinguishable particles can be classified into two groups based on their statistical behavior in large ensembles or based on the value of their intrinsic spin angular momentum. One group, known as bosons, has spin-angular momenta in integer multiples of the reduced Planck's constant $\hbar$. Examples include force-carrying particles like the photon. In fact, the photon is a boson that is its own antiparticle.

The other group of particles, known as fermions, have spin-angular momenta in half-integer multiples of $\hbar$. Matter-like particles such as the electron are examples of fermions that appear in elementary particle physics. An excitation that is formed at the TI superconductor boundary near a vortex of the superconductor has been predicted to give rise to a charge-neutral fermion. As of this writing, there is no conclusive proof that a fermionic excitation exists that is its own antiparticle, although there are several possible candidates.

It has been suggested that Majorana fermions at the interface of superconductors and TIs could be used as the basis for a qubit in a quantum computer.[34] The topological nature of the qubit means that it is non-localized and also robust against information loss from decoherence with the environment, overcoming one of the most pressing problems in quantum computing research.[8]

3.2.4. Image magnetic monopole

One exciting aspect of the magnetoelectric effect is the possibility of an electric charge near the topological surface inducing an image magnetic monopole, meaning that a magnetic field of the same form as that produced by a magnetic monopole can be produced.[29] Moreover, quasi-particles that are created from the interaction of an electric charge with its induced image monopole are particles with fractional statistics, obeying statistical rules intermediate between those of fermions and bosons.

By solving the equations of motion from the normal electromagnetic Lagrangian with the additional term $\Delta L = \theta(e^2/2\pi h)\boldsymbol{E}\cdot\boldsymbol{B}$, it can be shown that the in-plane component of the electric field created by an electric charge gives rise to the quantized Hall current,

$$j=P_3\frac{e^2}{h}\frac{q}{1+\alpha^2P_3^2}\frac{r}{(r^2+d^2)^{3/2}},$$

where r is the radial distance, and d is the distance from the electric charge to the interface.[29] This current gives rise to the magnetic field with the correct form representing a monopole. At this time, it should be pointed out that the magnetic flux still forms closed loops.

3.2.5. Topological contributions to the Faraday and Kerr effects

Recently, the magnetoelectric effect in topological insulators has been indirectly probed by studying the magneto-optic Kerr effect in thin films of the TI Bi_2Te_3 in an applied magnetic field using THz radiation.[30] The magneto-optic Kerr effect is a change in the polarization and intensity of reflected light from a magnetized surface. The effect is useful in the fundamental study of topological insulators as it gives a way to measure the effective mass of the surface states under broken time-reversal symmetry. However, using the magneto-optic Kerr effect in Bi_2Te_3 has not yet allowed for the quantized nature of the magnetoelectric effect to be observed. It is thought that the thin films must achieve higher carrier mobility and have a Fermi level that is tuned very close to the induced surface gap before the quantized nature will be observed.[35]

4. Synthesis of topological insulator nanostructures

4.1. Introduction

The exciting physics and potential applications of topological insulators have inspired a tremendous amount of work in making high-quality topological crystals such as TI thin films, bulk crystals, and nanostructures. Particularly, nanostructures from Bi_2Se_3, Bi_2Te_3, $(Bi_xSb_{1-x})_2Te_3$, $Bi_2(Se_xTe_{1-x})$, Sb_2Te_3, and Sb-doped Bi_2Se_3, have been synthesized and characterized. The methods for synthesizing TI nanostructures range from mechanical exfoliation from a bulk crystal to growing the nanostructures from vapors via a vapor–solid (VS) or vapor–solid–liquid (VLS) mechanism or in a solution that is heated or treated with ultrasonic sound.

A common method for growing TI nanostructures is a vapor–liquid–solid technique. The VLS technique is used to promote anisotropic crystal growth often by using metal nanoparticle catalysts. The technique can be broken down into three distinct stages, starting with alloying the metal with the vapor, followed by nucleation of the crystal, and finishing with axial growth.[36] The VLS technique can be implemented with a partially evacuated horizontal tube furnace that has an inert gas flowing through it. Typically, the source material is placed in a relatively warm region of the furnace and vapor is transported by the inert gas to a cooler region where a metal nanoparticle covered substrate is placed. The material can then be deposited on the substrate with the catalyst, helping to achieve nucleation of the nanostructure and uniaxial crystal growth.

However, for the synthesis of some nanostructures, such as Bi_2Se_3 nanoplates, it is possible to be grown directly on SiO_2/Si without using the metal catalyst. This altered technique is known as vapor–solid (VS) growth.

4.2. Bi_2Se_3 nanostructures

The binary compound Bi_2Se_3 is very popular for TI studies as it has a relatively large bandgap (~ 0.3 eV) compared with other TI compounds. Bi_2Se_3 crystallizes in a rhombohedral structure with space group $R\bar{3}m$. The structure can be thought of as consisting of five-layer stacks of Se–Bi–Se–Bi–Se, known as a quintuple layer (QL). The QLs are held together by the van der Waals dipole–dipole interaction and each QL is $\sim$1 nm thick. Due to the relatively weak attraction between atomic planes by the van der Waals interaction, thin nanoflakes of Bi_2Se_3 can be created by peeling off layers of the crystal by using Scotch tape until only a very thin film remains. The method is similar to the manual exfoliation technique used to create graphene.

When Bi_2Se_3 was synthesized for possible topological surface states, it was studied as a thermoelectric material, and nanobelts had been grown via a sonochemical technique and nanoplates by both solvothermal synthesis and by metal-organic chemical vapor deposition.[37]

In the sonochemical technique, ultrasonic irradiation in the frequency range from 20 kHz to 1 MHz can be used for chemical synthesis as it is known to speed up the rate of many chemical reactions and the ultrasonic radiation provides energy for the re-arrangement of the structural arrangement. The synthesis can be performed by dissolving bismuth chloride into deionized water which is then added to a selenious acid. The solution is kept at room temperature and stirred before adding diamine hydrate and then is irradiated with ultrasonic sound for 15 h. Using this method, nanobelts of 8–10 nm in thickness, 20–80 nm wide and several microns in length have been synthesized by the dissolution and crystallization of nanoflakes in this reactant solution.[38] In the solvothermal method for synthesis of thermoelectric Bi_2Se_3, $BiCl_3$ is dissolved in diethylene glycol before adding ammonia and stirring. Then, sodium sulfite and Se powder are added and the mixture is heated to 160 °C in a sealed chamber for 22 h. The produced hexagonal nanoflakes have typical edge lengths $\sim$ 300 nm and the growth direction is known to be $[10\bar{1}0]$.[39]

Recently, the VLS technique described earlier has been commonly used to grow high-quality Bi_2Se_3 crystals for the study of topological surface states. Using a Au catalyst, single-crystalline Bi_2Se_3 nanoribbons have been fabricated in this way,[26] using a horizontal tube furnace. Silicon [100] substrates were coated with Au nanoparticle catalysts by functionalizing with 0.1% w/v aqueous poly-L-lysine solution and then placing the sample in a colloid solution of 20-nm-diameter Au. The Bi_2Se_3 source material was placed in the warm central region of the tube furnace. Nanoribbons grew 6–10 cm away from the source under the conditions that the tube is evacuated to 30 mTorr and flushed with Ar before heating the source to 500 ° C and growth lasts 5 h under an Ar-rich base pressure

of 50 Torr. The grown nanoribbons had typical thicknesses of 25–100 nm and widths that could range from 50 nm to several microns.[26] The electron density of the nanoribbon can be altered by using a Sn/Au alloy as a catalyst to dope with Sn, controlling the growth temperature, or post-annealing the sample in Se vapor. For the grown samples, Hall effect measurements show the electron carrier density between 3×10^{13} cm^{-2} and 2×10^{14} cm^{-2}.

Bi_2Se_3 nanoplate synthesis has been carried out using a catalyst-free VS technique using a 12-in horizontal tube furnace. Source powder of Bi_2Se_3 is placed in the warm center of the tube furnace and oxidized Si wafers are placed $\sim$ 12 cm from the source. The furnace is pumped to a pressure of 100 mTorr and flushed with Ar prior to heating the source material to temperature of 460–500 °C while the pressure is held at 100 Torr for approximately 5 min before allowing the setup to cool down. The results of synthesis are ultrathin ($\sim$3–6 QL) nanoplates where the growth speed in the lateral direction is much faster than in the vertical thickness direction due to the bonding anisotropy.[37] The grown Bi_2Se_3 and Bi_2Te_3 were characterized by atomic force microscopy, as shown in Fig. 1.

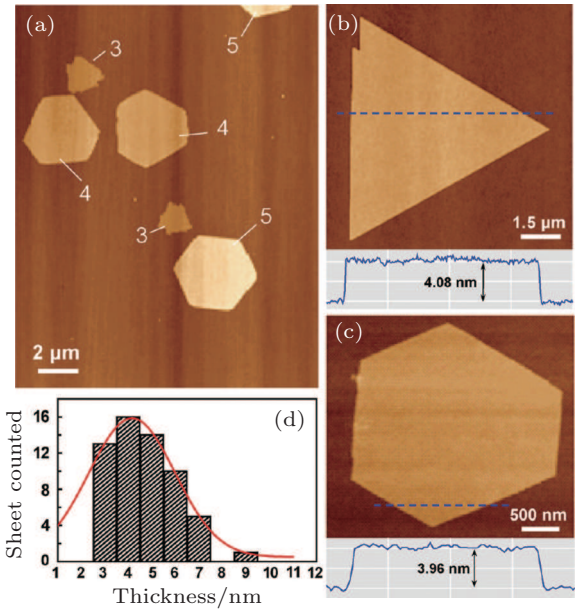


Fig. 1. Atomic force microscopy images of Bi_2Se_3 and Bi_2Te_3 nanoplates. (a) Large area image of Bi_2Te_3 nanoplates with the thickness of each indicated in units of QLs. (b) Image of a Bi_2Se_3 nanoplate with a height profile along the dashed line. (c) Image of a Bi_2Se_3 nanoplate with a height profile along the dashed line. (d) A Gaussian fit to the thickness distributions for grown Bi_2Te_3 nanoplates.[37]

More recently, Bi_2Se_3 nanoplate arrays have been successfully grown on mica via a catalyst-free VS technique in a 12-in horizontal tube furnace, following the previously described procedure.[40] In this way, the growth of nanoplates can be controlled both in orientation and position on the substrate. The obtained nanoplates have lateral dimensions up to $\sim$0.1 mm and thickness down to 1–2 nm. Angle-resolved photoemission spectroscopy (ARPES) performed on large nanoplate aggregates revealed a direct bulk gap and surface states with a single Dirac cone. The bulk conduction band was partially occupied, indicating the n-type doped nature. For electronic measurement a six-terminal Hall bar pattern was directly patterned on an individual nanoplate through a conventional photolithography technique and an Ohmic contact was obtained by thermal evaporation of Cr/Au (5 nm/50 nm). Room temperature transport property measurement indicated that the drain current responded linearly with the source-drain voltage with a four probe resistance of 7.4 kΩ.

Bi_2Se_3 has been identified as one of the most promising TI materials due to its simple surface state structure and relatively large bulk band gap ($\sim$ 0.3 eV), and synthesis of Bi_2Se_3 nanostructures has been successfully demonstrated. Unfortunately, these Bi_2Se_3 nanostructures are always n-type, owing to a large amount of Se vacancies in the crystal, leading to a metallic bulk conduction that overwhelms the surface transport. Tang *et al.* demonstrated the synthesis of pure Bi_2Se_3 nanoribbons in a horizontal tube furnace via the VLS mechanism with gold particles as catalysts, similar to the previously mentioned method.[26] To improve the quality of Bi_2Se_3 nanoribbons for surface state transport, they used Ar/H_2 (10%) as carrier gas instead of pure Ar gas. Magnetoresistance measurements on these Bi_2Se_3 nanoribbons under the perpendicular magnetic field showed a linear magnetoresistance response with the magnetic field, while when the magnetic field is parallel to the surface of nanoribbon, the magnetoresistance is almost negligible, indicating a pure two-dimensional (2D) transport, which verifies that the 2D topological surface state exists in bulk Bi_2Se_3. Angle-dependent SdH oscillations further suggest the existence of a 2D Fermi surface and 2D surface-state conduction. This linear magnetoresistance response is also robust at variant temperatures up to room temperature, suggesting the potential room temperature magneto-electronic applications of TI nanomaterials.

Exfoliation of Bi_2Se_3 nanoribbons has been accomplished using the cantilevered tip from atomic force microscopy (AFM) to break off layers of the nanoribbon into ultrathin nanoribbons of thickness ranging from 1 QL to 6 QL.[41] The thickness profiles for several exfoliated nanoribbons are given in Fig. 2. For ultra-thin Bi_2Se_3 nanoribbons, a surface energy gap exists for 1 QL and 2 QL samples due to the coupling of the top and bottom surface, but the gap is diminished above 2 QLs. For the grown nanoribbons before exfoliation, the measured resistance was found to decrease as the temperature goes down to 2 K, which is as expected, as the samples are usually heavily doped. For the 5-QL sample, the resistance increases as the temperature decreases, but it does not increase exponentially at low temperatures as is typical for band insulators.[41] It may be that the chemical potential remains near the bulk and surface gap as the outer 1–2 QLs on

each side are insulating due to surface chemistry.

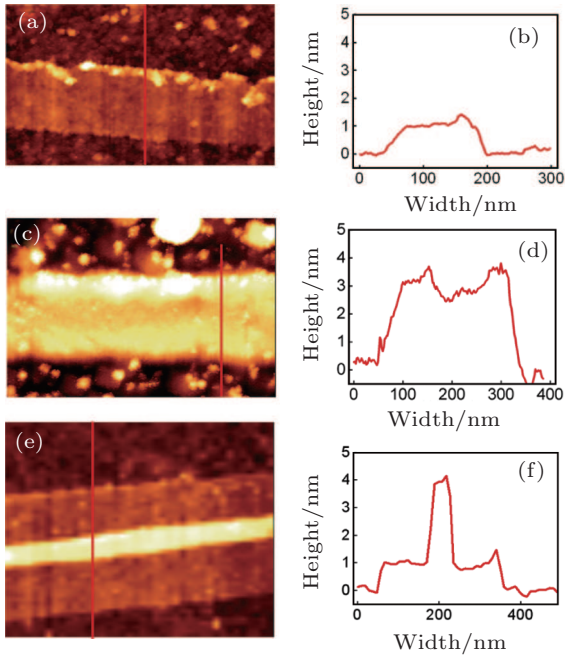


Fig. 2. AFM images of Bi_2Se_3 nanoribbons exfoliated by AFM. (a) and (b) Image and height profile along the red line for a 1 QL thick nanoribbon. (c) and (d) Image and profile for 3-QL-thick ribbon. (e) and (f) Image and profile for a 4-QL strip on a 1-QL-thick ribbon.[41]

For magnetic doping of nanostructures, the Au catalyst reported previously for nanoribbon growth can be replaced by a Ni–Au or Fe–Au catalyst where the Ni and Fe act as both magnetic impurities and as catalysts. In experiments, 5 nm of Au and 2 nm of the magnetic impurities Ni or Fe are deposited on Si [100].[42] The Au layer acts as a capping layer that helps prevent the oxidation of the magnetic impurities. Using energy dispersive X-ray spectroscopy (EDS) it was found that the catalyst particles at the top end of the nanoribbons contain the magnetic impurities, which suggests that some of these magnetic impurities are present in the nanoribbon as dopants. In order to confirm the presence of magnetic impurities in the ribbons, temperature-dependent resistance measurements were obtained on Fe-doped Bi_2Se_3 nanoribbon devices. For nanoribbons with no magnetic doping it was found that the resistance monotonically decreases as the temperature decreases, as seen in Fig. 3(a), down to $T \sim 30$ K, at which point the resistance saturates down to the lowest temperature measured of 2 K.[42]

For an Fe-doped nanoribbon, the resistance increases with decreasing temperature below ~ 30 K. Figure 3(b) shows the resistance of a Bi_2Se_3 nanoribbon down to 2 K. The scale for the solid curve is given on the left, while the scale for the dashed curve is on the right. The logarithmic increase of the resistance with decreasing temperature before saturating at 400 mK (Fig. 3(c)) is characteristic of the Kondo effect, which describes the scattering of electrons from magnetic impurities. Magnetoresistance measurements were also performed on both un-doped and Fe-doped Bi_2Se_3 nanoribbons. Weak antilocalization (WAL) was observed in un-doped ribbons due to the strong spin–orbit coupling. WAL is an effect that occurs in systems with spin–orbit coupling where the resistivity of a sample is lowered due to the destructive interference of two self-intersecting paths where the carriers move in opposite directions and therefore have different directions of spin due to the spin–orbit coupling. However, because of the presence of magnetic impurities, WAL is suppressed in the Fe-doped samples.[42]

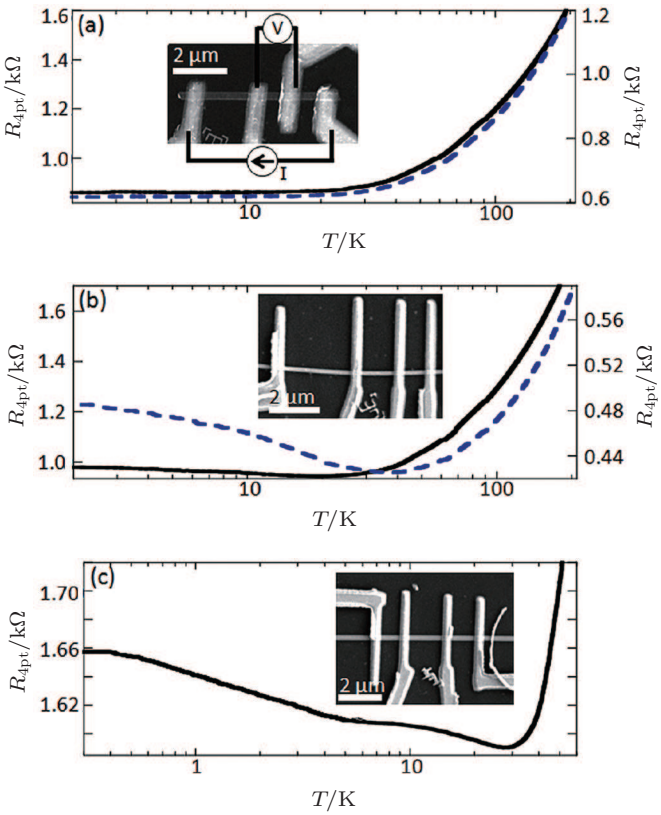


Fig. 3. Four-point resistance as a function of temperature of Fe-doped and undoped Bi_2Se_3 nanoribbons. The scale for the solid curve is given on the left, and the scale for the dotted curved is given on the right. The devices used in the measurements are shown in the insets. (a) Resistance for an undoped Bi_2Se_3 nanoribbon as a function of temperature down to 2 K. (b) Resistance as a function of temperature for an Fe-doped nanoribbon down to 2 K. (c) The four-point resistance for an Fe-doped nanoribbon down to 300 mK. The logarithmic increase in resistance below ~30 K is characteristic of the Kondo effect.[42]

4.3. Bi_2Te_3 nanostructures

Another TI material that is very similar to Bi_2Se_3 is Bi_2Te_3. It possesses the same crystal structure as Bi_2Se_3 with QL ~ 1 nm thick, and like Bi_2Se_3, it has previously been studied as a thermoelectric material. Since Bi_2Te_3 has a bandgap about half the size of that of Bi_2Se_3, Bi_2Se_3 is still the more popular compound for research.

Bi_2Te_3 nanoplates have been synthesized in the same catalyst-free method used for Bi_2Se_3 and described in the last section, except that the growth temperature is changed to 450–480 °C and the pressure during growth is 20 Torr. A standard

four-point probe with Ohmic contacts was fabricated on the nanoplates using e-beam lithography and thermal evaporation of 10 nm of Cr and 160 nm of Au. Al_2O_3 and a patterned Cr/Au top gate are then fabricated on top of the device.[37] Resistance measurements are then performed at 2 K in a physical property measurement system (PPMS). The response from gating indicates that the nanoplates are n-type due to antisite defects and Te vacancies.

The resistance of the nanoplate devices increases quasi-linearly as the gate voltage is increased from 0 to −17.5 V, as can be seen in Fig. 4(a). As the voltage is further reduced beyond −17.5 V, the rate of increase of resistance is again nearly constant but larger than in the region from 0 to −17.5 V. Hall measurements estimate the areal carrier density with zero gate bias to be 7.2×10^{13} cm^{-2} and 2.1×10^{13}cm^{-2} when the gate voltage is at −20 V.[37]

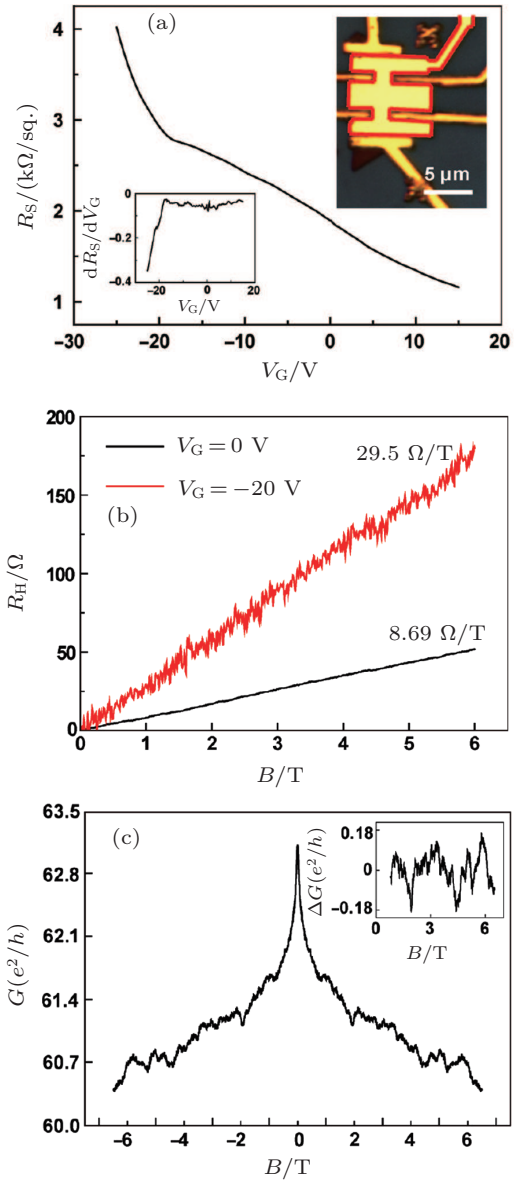


Fig. 4. Transport characteristics of a Bi_2Te_3 nanoplate. (a) Schematic of Hall bar fabricated on the nanoplate. (b) The channel resistance as a function of temperature. (c) The dependence of the channel resistance on gate voltage and temperature.[43]

To tune the Fermi level toward the middle of the bandgap and reduce bulk conductivity, Na-doped Bi_2Te_3 nanoplates have been synthesized by a solvothermal method.[43] The typical dimensions of a nanoplate are about 3–6 μm across and 35–50 nm thick. For measurements of transport properties, a six-terminal Hall bar was fabricated. A schematic of the device is shown in Fig. 5(a).

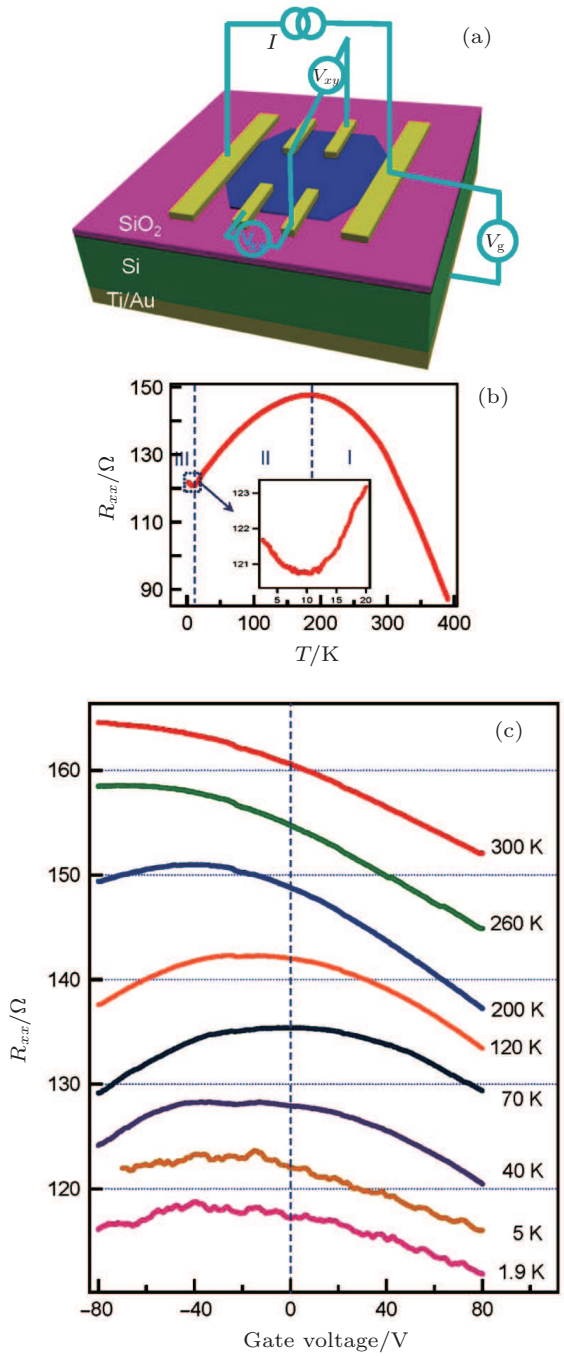


Fig. 5. Transport characteristics of a Bi_2Te_3 nanoplate. (a) Schematic of Hall bar fabricated on the nanoplate. (b) The channel resistance as a function of temperature. (c) The dependence of the channel resistance on gate voltage and temperature.[43]

The channel of the device was measured as a function of temperature (Fig. 5(b)) and three different temperature regimes were identified. From 2 K to 10 K, the resistance

increases as the temperature is lowered, due to the freeze out of carriers. From 10 K to 185 K, the channel exhibits metal-like behavior, as resistance rises with temperature. Finally, in the temperature range of 185–390 K, the channel acts like a semiconductor, as the resistance decreases with increasing temperature. Additional information can be gathered about the channel by varying the gate voltage.

Figure 5(c) shows the channel resistance as a function of gate voltage and temperature. At 1.9 K the channel shows n-type conduction for gate voltage between 0 and 80 V as the resistance is decreased by increasing gate voltage, while p-type conduction takes place for gate voltage between −80 V and −40 V. Around 40 K, the channel resistance is nearly constant from −40 V to 5 V. As the temperature rises above 40 K, the transition between n-type and p-type occurs at successively lower gate voltage until finally, near 300 K, the channel exhibits n-type conduction in the full voltage range from −80 V to 80 V.

Hall measurements were carried out on the nanoplate devices at 1.9 K. Figure 6 shows the total channel conductance G_{xy} as a function of magnetic field and gate voltage, where $G_{xy}=R_{xy}/(R_{xy}^2+R_s^2)$, and R_{xy} and R_s are the Hall and sheet resistances, respectively. We see that for an applied gate voltage of 0–40 V, the channel shows n-type behavior as the bulk hole contribution is outnumbered by the surface and conduction electrons. For −60 V and −80 V, the channel shows a p-type behavior, consistent with the data from Fig. 5(c).

Bi_2Te_3 nanoribbons have also recently been fabricated for use in studying the Aharonov–Bohm effect. The synthesis required that Bi_2O_2, Te, and ethylenediamine tetraacetic acid powders be added to a solution of polyvinylpyrrolidone dissolved in ethylene glycol prior to being stirred and sealed in a steel autoclave. The autoclave was heated in the temperature range of 180–220 °C for 4 h.[27] The ribbons grew along the $[11\bar{2}0]$ direction and were typically several hundreds of nanometers in width and several microns in length.

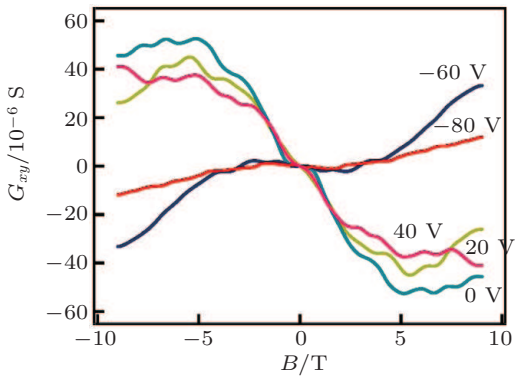


Fig. 6. The conductance versus magnetic field for a Bi_2Te_3 nanoplate FET for varying gate voltage. An n-type to p-type transition is observed by tuning the gate voltage.[43]

Since Bi_2Te_3 has the same type of structure as Bi_2Se_3 with QLs bonded by the van der Waals force, nanoflakes of Bi_2Te_3 can easily be exfoliated from a bulk crystal with the use of Scotch tape. After exfoliating flakes on the tape, the tape is pressed against a cleaned SiO_2/Si substrate with tweezers and the flake will remain on the substrate as long as the tape is peeled away slowly.[44] Using atomic force microscopy, the nanoflakes were found to have a characteristic size from less than 1 micron to around 100 microns and thicknesses from 10 nm to 100 nm. After making electrical contacts using e-beam lithography, the sheet resistance $R_\square$ was measured using the van der Pauw method, and Hall measurements were obtained at 300 K.[44] The hole density was found to be 1.6×10^{19} cm^{-3} with a mobility of 210 cm$^2/(\mathrm{V}\cdot\mathrm{s})$ for a 140-nm-thick sample, which is about half the mobility reported from a bulk sample. Nanotubes of Bi_2Te_3 have also been grown with the technique of galvanic displacement. In this technique, Ni nanowires can be immersed in an acidic nitric solution that contains within it Bi^{3+} and $HTeO_2^+$ ions. Due to the difference in reduction potentials, the Ni nanowires are galvanically displaced to form Bi_2Te_3.[45]

4.4. $(Bi_xSb_{1-x})_2Te_3$ nanostructures

Aside from the widely studied binary TI compounds, ternary compounds have been used as a way to better control the bulk conductivity. Cui *et al.* have grown single-crystalline $(Bi_xSb_{1-x})_2Te_3$ nanoplates on 300-nm SiO_2 surface of a Si wafer with a catalyst-free VS growth using Bi_2Te_3 and Sb_2Te_3 powders as precursors. By tuning the chemical composition, the lowest intrinsic carrier density is achieved for the compound $(Bi_{0.50}Sb_{0.50})_2Te_3$. However, the doping can be affected by the external environment, where, for example, water can act as an n-type dopant.[46] The topological surface states of the compound were verified by using ARPES on the (0001) plane of $(Bi_xSb_{1-x})_2Te_3$ bulk crystals of varying compositions. Experimental and theoretical data suggest topological surface states across the entire compositional range of Bi/Sb ratios.

Using back-gated FET devices the resistance and Hall coefficient can be found under varying gate voltages. As the gate voltage is swept for very thin (∼ 5 nm) nanoplates, the resistance is found to have a maximum spike about 50 times as large as the nearly constant resistance at positive gate voltage. The Hall coefficient changes sign at the point of maximum resistance, suggesting an ambipolar field effect where the nanoplate can be tuned between n-type and p-type under the influence of a gate bias.

The effects of temperature on the ambipolar effect in these nanoplates have also been studied. In the electron-conducting region the resistance decreases with decreasing temperature, due to suppressed electron–phonon scattering. When the gating is adjusted to put the nanoplate in a state with a mixture of electron and hole carriers, the resistance increases

with decreasing temperature in the range of 2 K to 120 K due to the freeze out of carriers.[46]

4.5. $Bi_2(Se_xTe_{1-x})_3$ nanostructures

Another confirmed ternary TI compound is $Bi_2(Se_xTe_{1-x})_3$. As with the compound $(Bi_xSb_{1-x})_2Te_3$, $Bi_2(Se_xTe_{1-x})_3$ is studied as the composition can be tuned to lower the total bulk carrier density. Work has been carried out by Cui *et al*. regarding weak antilocalization (WAL) in nanoribbons and nanoplates of $Bi_2(Se_xTe_{1-x})_3$.[47]

The nanoribbons were grown using a 10-nm gold film as the metal catalyst using the VLS technique in a tube furnace with Bi_2Se_3 and Bi_2Te_3 powders as the precursors. By varying the relative portions of the two source materials, the bulk carrier concentration can be tuned. After flushing the tube with Ar at 100 mTorr, the furnace is heated to 500 ° C and held for $\sim$ 2 h with an Ar flow of 30–150 standard cubic centimeters (sccm). For the compound $Bi_2(Se_xTe_{1-x})_3$, the carrier density in the nanoribbon was seen to decrease with x. Since the carrier density is lower for the nanoribbons than for nanoplates for a given x, nanoribbons were focused on in transport experiments.[47] The carrier density for $Bi_2(Se_xTe_{1-x})_3$ is roughly around 10^{19} cm^{-2}.

A six-terminal Hall bar was constructed using e-beam lithography and thermal evaporation of Cr/Au for metal contacts. From Hall measurements done at 2 K on $Bi_2(Se_{0.34}Te_{0.66})_3$, the two-dimensional carrier density is n_{2D}= 1.69$\times 10^{14}$ cm^{-2} and the Hall mobility is 28 cm^2/Vs, which is much lower than the mobility in Bi_2Se_3 bulk or nanostructure samples. The resistance increased as the temperature was lowered, which is unusual for such a highly doped material.

WAL is a correction to the classical magnetoresistivity which lowers its expected value and is caused by the wave nature of the electron. In experiments, the magnetoconductance of a wide nanoribbon was obtained by tilting the ribbon relative to a magnetic field from a grazing angle to direct incidence of the field. The contribution that the surface electrons make to WAL should depend only on the sine of the angle between the surface and the magnetic field.[47]

The nanoplates were grown in a similar fashion to the nanoribbons except that the growth is directly on SiO_2, the growth temperature is 480 °C, and it is held there for 10 min. The conclusions drawn from the study of the nanoribbons can also be applied to the nanoplates, except that the plates have a much higher carrier density.

4.6. Sb-doped Bi_2Se_3 nanostructures

One of the main obstacles in current TI research regarding surface state transport properties is the bulk charge carriers outnumbering the surface state electrons owing to materials imperfection issues, such as Bi_2Se_3 is always heavily-doped n-type due to excessive Se vacancies, and Bi_2Te_3 is p-type due to the presence of anti-site defects between Bi and Te atoms. As introduced above, ternary compounds TI, such as $(Bi_xSb_{1-x})_2Te_3$ and $Bi_2(Se_xTe_{1-x})_3$, showed improved surface transport characteristics compared with their binary counterparts.[46,47] Recently, Cui *et al.* demonstrated another effective way to suppress bulk transport, which is doping. Sb-doped Bi_2Se_3 nanoribbons have been successfully synthesized in a horizontal tube furnace via VLS growth using a silicon wafer substrate coated with thermally grown 10-nm-thick Au film. The source material of Bi_2Se_3 powder was placed into the center of the furnace, the doping source material of Sb_2Se_3 was placed upstream at a lower temperature zone, and the substrate was placed in a downstream zone. By varying the doping source powder's temperature, which can be achieved by placing the powder at different locations of the upstream zone in the tube furnace, the concentration of Sb dopant can be controlled. At a high Sb-doping level (6–7 atom%), the bulk carrier concentration can be reduced to $\sim 10^{13}$ cm^{-3}, and corresponding surface electron density near the bulk conduction band edge can also reach ~10^{13} cm^{-3}, suggesting the surface-dominant transport nature in Sb-doped Bi_2Se_3 nanoribbons. The effect of doping concentration on surface-state transport was further manifested by applying an electrostatic gate. High doping concentration showed a large gate response and a significant decrease in bulk carrier concentration. Another factor degrading TI materials' performance is environmental contamination. Several studies have observed that exposure to H_2O and O_2 atmosphere will generate addition bulk carriers in TI materials.[37] To eliminate this effect, Cui *et al*. capped Sb-doped Bi_2Se_3 nanoribbons with a 15-nm-thick ZnO layer. The gate dependent transport properties indicated that the Fermi level is very close to the Dirac point and the carrier density was further decreased to 5×10^{12} cm^{-3}, suggesting a surface state dominated transport process.[41]

4.7. Sb_2Te_3 nanostructures

Sb_2Te_3 is the final TI nanostructure system that we will discuss. Just as for other materials, Sb_2Te_3 nanostructures have been synthesized using an Au-catalyzed VLS growth method. Nanoparticles of Au were immobilized on SiO_2/Si by a thin layer of polyelectrolyte. Elemental powders of Sb and Te were heated up in a tube furnace under Ar gas flow with the Sb powder placed at the center of the hot zone, the Te 13.5 cm upstream of the Sb, and the Au covered substrates downstream from the precursors.[48] The best location for nanostructure growth was found to be 9–11 cm downstream from the Sb. The type of nanostructure produced varied with the growth conditions. Nanoplates could be grown without the gold catalyst at 430 °C and 80 sccm air flow and typically had

micron sized edge lengths and were several hundred nanometers thick. Nanowires appear with temperature in the vicinity of ~ 430 °C and flow rate of 80 sccm. By raising the flow rate to 140 sccm, thicker nanobelts of typical widths around ~ 250 nm can be produced.[48]

Transport properties measurements of Sb_2Te_3 nanowires with different diameters at room temperature did not show a strong diameter-dependence, while at low temperature (below 50 K), the resistance of a nanowire with small diameter ($<$ 45 nm) increases to several times the room temperature value. Magnetoresistance measurements of these Sb_2Te_3 nanowires showed the perpendicular magnetoresistance is parabolically dependent on the magnetic fields up to ± 10 T at all temperature regimes. However, due to the low mobility of the sample, Shubnikov–de Hass oscillation was not detected, and signatures of topological surface states were not observed either, because the Fermi level is deep in bulk valence band away from the gap.[49]

The experiments conducted concerning Sb_2Te_3 nanostructures.[48] focused on the ability to use nanowires of the compound as phase-change memory, namely, by applying a voltage pulse, the wire could be made amorphous and then be made to recrystallize. The change in resistance can be used for a memory device. More experimental work must be done on Sb_2Te_3 nanostructures to see if they might provide any advantages over other materials in TI research.

5. Characterization of topological insulator nanostructures

5.1. Introduction

Due to the lower volume-to-surface area ratio in TI nanostructures, several different types of quantum oscillations can be observed coming from the surface states that cannot be observed in bulk TI samples. The two effects that are often used feature a magnetic field dependent resistance oscillation. However, each of these magnetoresistance oscillation effects has different origins and so each will be talked about in turn.

5.2. Aharonov–Bohm effect

The Aharonov–Bohm (AB) effect, first predicted by Ehrenberg and Siday in 1949,[50] has been of significant interest to physicists, as it seems to cause problems with formulating Maxwell's equations as a gauge theory by elevating the electromagnetic potential to a real "physical" quantity instead of a computational tool for finding the electromagnetic field. The most common description of the AB effect is of the wavefunction of a charged particle that is moving around a solenoid to have its phase shifted by magnetic flux passing along the axis of the solenoid even if the magnetic field has a value of zero everywhere where the particle's wavefunction is non-negligible. The mechanism that accounts for the effect is a coupling between the electromagnetic potential and the phase of the wavefunction.

The effect is interesting from a physical prospective because, as noted earlier, the gauge invariance of Maxwell's equations imply that there should be an infinite number of different electromagnetic potentials describing the same "physical" electromagnetic field, while the AB effect seems to imply that there is a unique electromagnetic potential that is actually a physical quantity, as it couples with the wavefunction phase. The effect has been used to help study the surface states of topological insulators ,as the phase shift induced on the surface electrons in a TI by a magnetic field will cause periodic changes in the conductivity of the surface as the magnetic flux passing through the material is changed.[51]

In actual experiments, Bi_2Se_3 nanoribbons have been used to study the surface states via the AB effect as a nanoribbon can, more than a bulk sample or thin film, look much like a solenoid, and the AB effect in solenoids has been well studied. In the experiments a magnetic field is applied along the long axis of a Bi_2Se_3 nanoribbon that has been equipped with a four-point probe device with Ti/Au ohmic contacts. The magnetoresistance can then be measured using a physical property measurement system (PPMS).

The dominant frequency at which the resistance oscillates is given by $\Delta B = \Phi_0/A$ where A is the cross-sectional area of the nanoribbon and $\Phi_0 = h/e$ is the flux quantum where h is Planck's constant. There is also a weaker higher order harmonic oscillation where the flux is given by $h/2e$. Cui *et al.* have reported on the AB effect magnetoresistance oscillations of a Bi_2Se_3 nanoribbon by measuring the resistance when the applied magnetic field is in the range of -9 T to 9 T. It was found that the dominant oscillation frequency was $\Delta B = 0.62$ T, while the measured cross-sectional area of a nanoribbon was found to be $A = 6.6\times10^{-15}$ m^2. These measurements produce an estimate for h/e to be roughly 4.09×10^{-15} Tm^2, which differs from the best estimates of h/e by about 1% . In the same experiment, the effect of the temperature on the oscillation amplitude was observed and it was found that most of the oscillatory behavior was present up to 20 K.[26]

Now, there are two different values of the magnetic flux that do not break time-reversal symmetry on the TI surface, and $h/2e$. However, these two cases are not identical, as the Dirac point at the surface should exist only for flux of $h/2e$.[51] There are also ways other than the AB effect to search for the existence of nontrivial Berry phase, including weak antilocalization, which can be triggered by both spin–orbit coupling and the helicity of the surface state in topological insulators.

In actual experiments on Bi_2Se_3 nanowires, the weak antilocalization-induced $h/2e$ oscillation is almost absent while the maximum conductance, surprisingly, is present

when the magnetic flux is zero. More recently, an angle-dependent magnetoconductance study on $Bi_2(Se_xTe_{1-x})_3$ nanoribbons and nanoplates clearly revealed the weak antilocalization effect despite the high electron density ($\sim 10^{19}$ cm^{-3}). Power law dependence of the dephasing length on temperature reflects the two-dimensional (2D) nature of weak antilocalization effect, and the weak antilocalization's origin in topological surface states can be verified by the fit to the 2D localization theory.[47]

5.3. Shubnikov–de Haas oscillations

The use of Shubnikov–de Haas (SdH) oscillations for studying surface states in TI is much like using AB oscillations in many ways. Similar to AB oscillations, periodic changes in the magnetoresistance are measured in order to extract information about the surface states. The origin of the periodic change in magnetoresistance, however, is different in the SdH effect.

When exposed to a magnetic field normal to the surface, the Dirac surface states of a TI are quantized into Landau Levels (LLs). The energy of the levels is given by

$$E_n = v_F\sqrt{2n\hbar eB},$$

where v_F is the Fermi velocity, n is an integer known as the LL index, $\hbar$ is the reduced Planck's constant, e is the electric charge, and B is the magnetic field. The conductance of the sample changes periodically as the magnetic field is increased because the Fermi level moves across various quantized LLs, leading to peaks in conductivity when the Fermi level is at the midpoint of an LL, and reaching a minima when it lies between two LLs.[52]

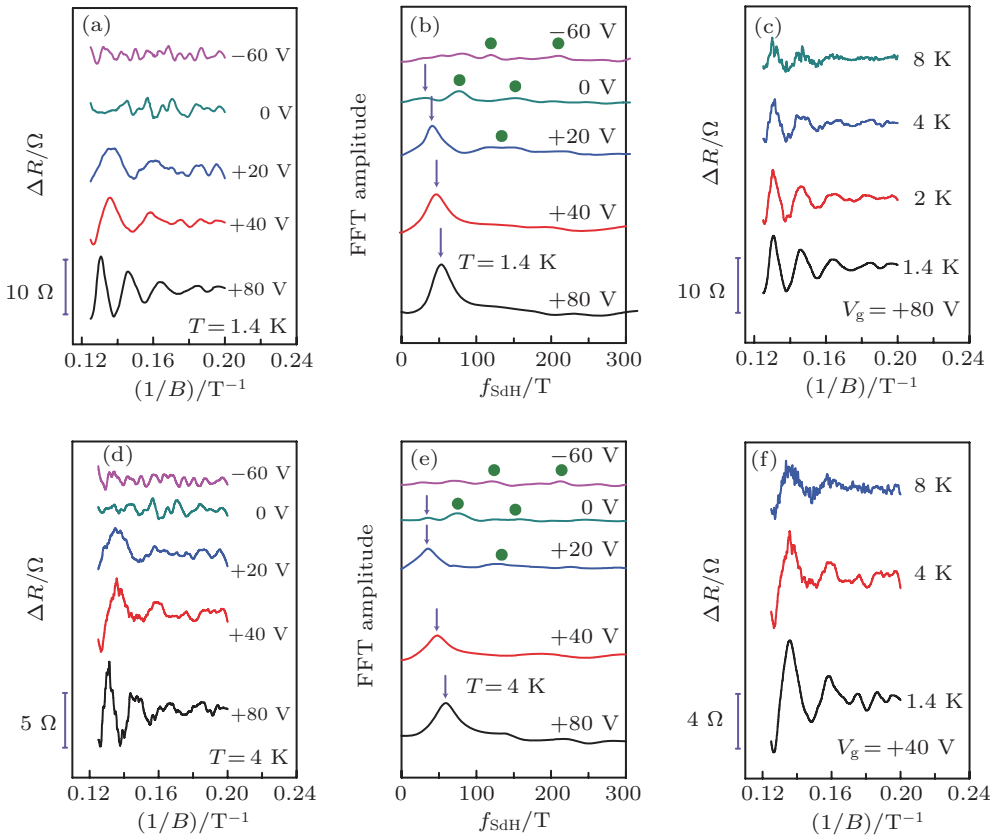


Fig. 7. SdH oscillations from a Bi_2Te_3 nanoribbon. Magnetoresistance measurements made at 1.4 K (a) and 4 K (d) at a variety of gate voltages. Fast Fourier transform spectra for samples at 1.4 K (b) and 4 K (e). Temperature dependence of SdH oscillations for gate voltages of +80 V (c) and +40 V (f).[27]

SdH oscillations in a back-gated Bi_2Te_3 nanoribbon have been studied at low temperature under a variety of gate voltages.[27] A field-effect transistor device is fabricated on a SiO_2 layer of a p^{++} Si substrate with a Ti/Au electrode as the back-gate. At 1.4 K, the magnetoresistance shows no SdH oscillations under zero gate bias (Fig. 7). The hole carriers are partially depleted and the bulk begins to conduct less when a positive gate voltage is applied. As a result, SdH oscillations in the magnetoresistance are seen to grow in amplitude as the gate voltage is swept from +20 V to +80 V as shown in Fig. 7(a). Under a negative bias, holes are induced in the bulk, leading to no discernible signal from SdH oscillations of the surface states. The same results are obtained at 4 K except the amplitudes of the SdH oscillations are diminished.

After measuring the magnetoresistance, additional parameters can be calculated, including the transport lifetime τ, mean free path $l = V_F\tau$, and mobility $\mu = e\tau/m_{cycl} = el/\hbar k_F$ by obtaining the best fit of

$$\log\left[\frac{\Delta R}{R_0}B\sinh\lambda(T)\right] \approx \frac{2\pi^2 E_F}{\tau e B V_F^2},$$

where ΔR is the magnetoresistance, B is the magnetic field, $\lambda(T) = 2\pi^2 k_B T m_{cycl}$ with k_B being the Fermi vector, T being the temperature, m_{cycl} being the cyclotron mass, and E_F and V_F being the Fermi energy and Fermi velocity, respectively. The factor $\lambda(T)$ can be found from temperature-dependent conductivity measurements as $\lambda(T)/\sinh\lambda(T) = \Delta\sigma_{xx}(T)/\Delta\sigma_{xx}(0)$, where $\Delta\sigma_{xx}(T)$ is the change in conductivity at temperature T. For Bi_2Te_3 nanoribbons the estimated values of these parameters are $l = 114$ nm and 160 nm, $\mu \sim 4560$ cm^2/Vs and ~ 5790 cm^2/Vs, and $\tau \sim 3.1\times10^{-13}$ s and $\sim 4.3\times10^{-13}$ s for a gate voltages of +40 V and +80 V, respectively.

6. Summary and perspective

Topological insulators are a recently discovered class of materials with a bulk energy gap and gapless spin-helical Dirac surface states that are protected by time-reversal symmetry. The surface states are characterized by carriers that have their spin locked to the direction of momentum and that dissipate little energy, as "U"-turn scattering is suppressed. The breaking of time-reversal symmetry gives mass to the surface carriers and plays an essential role in many different effects predicted to exist with TIs that could be useful for spintronics applications, such as the magnetoelectric effect, which allows for an applied electric field to generate a parallel-oriented magnetic field and vice versa.

Nanostructures are important in TI research, as nanostructured materials reduce the overall bulk contribution, allowing for easier study of the exotic surface states. Bi_2Se_3, Bi_2Te_3, $(Bi_xSb_{1-x})_2Te_3$, $Bi_2(Se_xTe_{1-x})$, Sb_2Te_3 and Sb-doped Bi_2Se_3nanostructures have all been grown using the VS or VLS method in a tube furnace. Bi_2Se_3 is a popular material due to its large bandgap and simple band structure, while the ternary compound materials have the advantage of tunable carrier density. Mechanical exfoliation from a bulk crystal with Scotch tape to make nanoflakes is also possible in these materials due to the weak van der Waals interaction holding together atomic planes. Magnetic doping of nanostructures has been accomplished by allowing a magnetic material like Fe to be added to the metal catalyst used in the growth of nanowires and nanoribbons.

Magnetoresistance oscillations via the AB effect and SdH oscillations are used to extract information about the surface states. With the AB effect, the periodic resistance change with respect to applied magnetic field is due to interference effects of the surface carriers. With SdH oscillations, magnetoresistance oscillations are brought about by the populating and depopulating of quantized Landau levels. Both of these types of oscillations have been observed in nanoribbons of TI materials. Using data obtained from magnetoresistance measurements, the transport lifetime, mean free path, and mobility can be calculated.

Although a surge of interest and research activities in topological insulators has been envisioned in recent years, new physical phenomena arising from the unique topological surface states remain elusive. One of the intriguing challenges is the undesirable bulk carriers caused by overwhelming defect formation during the growth process. The relatively small bandgaps in the well-known TIs seem to further complicate the multiple-channel conduction issue, as bulk conduction is very sensitive to defects and doping. The TI nanostructures, however, to some extent have helped reveal the surface states because of large surface-to-volume ratios, although a 100% pure surface conduction remains challenging. One of the future research innovations could be the exploration of topological heterostructures involving topological insulators and other materials such as magnetic and superconducting materials, where proper proximity effects in the interface take place with the surface states. The special spin (transport) properties of the surface states can be also manipulated using some special structures involving magnetic oxides as gate dielectrics. In summary, the recent advances in the physics of topological insulators have been led by the initial theoretical breakthroughs and the subsequent verification from experiments. The unusual metallic surfaces of these insulators may lead to a discovery of unknown but rich physics and new spintronic/electronic devices.

References

[1] Moore J 2009 *Nat. Phys.* **5** 378
[2] Zhang H, Liu C X, Qi X L, Dai X, Fang Z and Zhang S C 2009 *Nat. Phys.* **5** 438
[3] McIver J, Hsieh D, Steinberg H, Jarillo-Herrero P and Gedik N 2011 *Nat. Nanotech.* **7** 96
[4] Chen Y, Analytis J, Chu J H, Liu Z, Mo S K, Qi X L, Zhang H, Lu D, Dai X and Fang Z 2009 *Science* **325** 178
[5] Manoharan H C 2010 *Nat. Nanotech.* **5** 477
[6] Moore J E 2010 *Nature* **464** 194
[7] Chen Y, Chu J H, Analytis J, Liu Z, Igarashi K, Kuo H H, Qi X, Mo S K, Moore R and Lu D 2010 *Science* **329** 659
[8] Hasan M Z and Kane C L 2010 *Rev. Mod. Phys.* **82** 3045
[9] Wilczek F 1987 *Phys. Rev. Lett.* **58** 1799
[10] Qi X L and Zhang S C 2010 *Phys. Today* **63** 33
[11] Qi X L, Hughes T L and Zhang S C 2008 *Phys. Rew. B* **78** 195424
[12] Nussinov Z and Ortiz G 2009 *Ann. Phys.* **324** 977
[13] Klitzing K V, Dorda G and Pepper M 1980 *Phys. Rev. Lett.* **45** 494
[14] Hsieh D, Qian D, Wray L, Xia Y, Hor Y S, Cava R and Hasan M Z 2008 *Nature* **452** 970
[15] Kane C and Moore J 2011 *Phys. World* **24** 32
[16] Shao H, Zhou X, Li Y, Liu G and Zhou G 2011 *Appl. Phys. Lett.* **99** 153104
[17] Munkres J R 2000 *Topology* (2nd edn.) (Upper Saddle River: Prentice Hall)

[18] Bernevig B A, Hughes T L and Zhang S C 2006 *Science* **314** 1757
[19] König M, Wiedmann S, Brüne C, Roth A, Buhmann H, Molenkamp L W, Qi X L and Zhang S C 2007 *Science* **318** 766
[20] Qu D X, Hor Y, Xiong J, Cava R and Ong N 2010 *Science* **329** 821
[21] Analytis J G, Chu J H, Chen Y, Corredor F, McDonald R D, Shen Z and Fisher I R 2010 *Phys. Rev. B* **81** 205407
[22] Xia Y, Qian D, Hsieh D, Wray L, Pal A, Lin H, Bansil A, Grauer D, Hor Y and Cava R 2009 *Nat. Phys.* **5** 398
[23] Hsieh D, Xia Y, Qian D, Wray L, Dil J, Meier F, Osterwalder J, Patthey L, Checkelsky J and Ong N 2009 *Nature* **460** 1101
[24] Bianchi M, Guan D, Bao S, Mi J, Iversen B B, King P D and Hofmann P 2010 *Nat. Commun.* **1** 128
[25] Taskin A, Ren Z, Sasaki S, Segawa K and Ando Y 2011 *Phys. Rev. Lett.* **107** 016801
[26] Peng H, Lai K, Kong D, Meister S, Chen Y, Qi X L, Zhang S C, Shen Z X and Cui Y 2009 *Nat. Mater.* **9** 225
[27] Xiu F, He L, Wang Y, Cheng L, Chang L T, Lang M, Huang G, Kou X, Zhou Y and Jiang X 2011 *Nat. Nanotech.* **6** 216
[28] Vishveshwara S 2011 *Nat. Phys.* **7** 450
[29] Qi X L, Li R, Zang J and Zhang S C 2009 *Science* **323** 1184
[30] Aguilar R V, Stier A, Liu W, Bilbro L, George D, Bansal N, Wu L, Cerne J, Markelz A and Oh S 2011 arXiv:1105.0237
[31] Yu R, Zhang W, Zhang H J, Zhang S C, Dai X and Fang Z 2010 *Science* **329** 61
[32] Franz M 2010 *Science* **329** 639
[33] Nomura K and Nagaosa N 2011 *Phys. Rev. Lett.* **106** 166802
[34] Sarma S D, Freedman M and Nayak C 2006 *Phys. Today* **59** 32
[35] Tse W K and MacDonald A 2010 *Phys. Rev. Lett.* **105** 057401
[36] Wu Y and Yang P 2001 *J. Am. Chem. Soc.* **123** 3165
[37] Kong D, Dang W, Cha J J, Li H, Meister S, Peng H, Liu Z and Cui Y 2010 *Nano Lett.* **10** 2245
[38] Cui H, Liu H, Wang J, Li X, Han F and Boughton R 2004 *J. Cryst. Growth* **271** 456
[39] Wang D, Yu D, Mo M, Liu X and Qian Y 2003 *J. Cryst. Growth* **253** 445
[40] Li H, Cao J, Zheng W, Chen Y, Wu D, Dang W, Wang K, Peng H and Liu Z 2012 *J. Am. Chem. Soc.* **134** 6132
[41] Hong S S, Kundhikanjana W, Cha J J, Lai K, Kong D, Meister S, Kelly M A, Shen Z X and Cui Y 2010 *Nano Lett.* **10** 3118
[42] Cha J J, Williams J R, Kong D, Meister S, Peng H, Bestwick A J, Gallagher P, Goldhaber-Gordon D and Cui Y 2010 *Nano Lett.* **10** 1076
[43] Wang Y, Xiu F, Cheng L, He L, Lang M, Tang J, Kou X, Yu X, Jiang X and Chen Z 2012 *Nano Lett.* **12** 1170
[44] Luo J, Late D, Wu I, Biswas K, Kanatzidis M and Grayson M 2011 *AIP Conf. Proc.* **1416** 135
[45] Xiao F, Yoo B, Lee K H and Myung N V 2007 *J. Am. Chem. Soc.* **129** 10068
[46] Kong D, Chen Y, Cha J J, Zhang Q, Analytis J G, Lai K, Liu Z, Hong S S, Koski K J and Mo S K 2011 *Nat. Nanotech.* **6** 705
[47] Cha J J, Kong D, Hong S S, Analytis J G, Lai K and Cui Y 2012 *Nano Lett.* **12** 1107
[48] Lee J S, Brittman S, Yu D and Park H 2008 *J. Am. Chem. Soc.* **130** 6252
[49] Zuev Y M, Lee J S, Galloy C, Park H and Kim P 2010 *Nano Lett.* **10** 3037
[50] Ehrenberg W and Siday R 1949 *Pro. Phys. Soc. B* **62** 8
[51] Bardarson J H, Brouwer P and Moore J 2010 *Phys. Rev. Lett.* **105** 156803
[52] Xiong J, Luo Y, Khoo Y, Jia S, Cava R and Ong N 2012 *Phys. Rew. B* **86** 045314